HHS Public Access

Author manuscript

*J Endocrinol*. Author manuscript; available in PMC 2018 October 01.

Published in final edited form as:

*J Endocrinol*. 2017 October ; 235(1): 27–38. doi:10.1530/JOE-17-0289.

# Stress-responsive HILPDA is necessary for thermoregulation during fasting

**Matthew J. VandeKopple**[1], **Jinghai Wu**[1], **Lisa A. Baer**[2], **Naresh C. Bal**[3,5], **Santosh K. Maurya**[3,6], **Anuradha Kalyanasundaram**[3], **Muthu Periasamy**[3,6], **Kristin I. Stanford**[2], **Amato J. Giaccia**[4], **Nicholas C. Denko**[1,7], and **Ioanna Papandreou**[1,7,*]

[1]Department of Radiation Oncology, The Ohio State University, Columbus, Ohio, 43210

[2]Dorothy M. Davis Heart and Lung Research Institute; Department of Physiology and Cell Biology, The Ohio State University, Columbus, Ohio, 43210

[3]Department of Physiology and Cell Biology, The Ohio State University, Columbus, Ohio, 43210

[4]Department of Radiation Oncology, Stanford University, Stanford, CA 94305

## Abstract

Hypoxia-Inducible Lipid-Droplet Associated protein (HILPDA) has been shown to localize to lipid droplets in nutrient responsive cell types such as hepatocytes and adipocytes. However, its role in the control of whole-body homeostasis is not known. We sought to measure cell-intrinsic and systemic stress responses in a mouse strain harboring whole body Hilpda deficiency.

We generated a genetically engineered mouse model of whole body HILPDA deficiency by replacing the coding HILPDA exon with Luciferase. We subjected the knockout animals to environmental stresses and measured whole-animal metabolic and behavioral parameters. Brown adipocyte precursors were isolated and differentiated in vitro to quantify the impact of HILPDA ablation in lipid storage and mobilization in these cells.

HILPDA knockout animals are viable and fertile, but show reduced ambulatory activity and oxygen consumption at regular housing conditions. Acclimatization at thermoneutral conditions abolished the phenotypic differences observed at 22°C. When fasted, HILPDA KO mice are unable to maintain body temperature and become hypothermic at 22°C, without apparent abnormalities in blood chemistry parameters or tissue triglyceride content. HILPDA expression was upregulated during adipocyte differentiation and activation in vitro, however, it was not required for lipid droplet formation in brown adipocytes. We conclude that HILPDA is necessary for efficient fuel utilization suggesting a homeostatic role for Hilpda in sub-optimal environments.

[*]Corresponding address: Ioanna Papandreou, Department of Radiation Oncology, 420 W.12th Ave. The Ohio State University, Columbus, OH 43210. ioanna.papandreou@osumc.edu Phone: +1 614 3663906.

[5]Present address: School of Biotechnology, KIIT University, Bhubaneswar, India

[6]Present address: Sanford Burnham Prebys Medical Discovery Institute at Lake Nona, Orlando, Florida 32827

[7]N.D. and I.P. contributed equally to this work

**Declaration of Interest**

The authors have no conficts of interest to disclose.

**Keywords**

Hig2; Hypoxia; Lipid Droplets; Hypothermia

## Introduction

Lipid droplets (LDs) are emerging as very dynamic organelles that store lipids and participate in a number of biological processes (Fujimoto and Parton 2011). LDs consist of a hydrophobic core containing mainly triacylglycerols and steryl esters, surrounded by a phospholipid monolayer that is decorated with proteins (Goodman 2008). It is estimated that 50–200 proteins localize to the LDs surface (Krahmer, et al. 2013). Some LD associated proteins are involved in lipid metabolism, however, there are also enzymes and regulatory proteins that do not have recognized functions related to lipids. The LD proteome is very dynamic and is thought to depend on the needs for the cell type- or even LD-type to balance lipid storage and hydrolysis (Hsieh, et al. 2012). The most abundant LD proteins belong to the perilipin (PLIN) family of PAT-domain containing proteins. All 5 PLINs can coat LDs, and mouse models of *Plin* deficiency show similar and distinct phenotypes (Sztalryd and Kimmel 2014). For example, PLIN1 is most highly expressed in white and brown fat and steroidogenic tissues, whereas PLIN2 and PLIN3 are ubiquitously expressed (Sztalryd and Kimmel 2014). PLIN1 coats the adipocyte LDs and controls basal and stimulated lipolysis. Under basal conditions it inhibits access of cytosolic lipases to the triacylglycerol core, whereas upon stimulation by β-adrenergic signaling cAMP levels rise, activated Protein Kinase A (PKA) phosphorylates PLIN1, which recruits Adipose Triglyceride Lipase and Hormone Sensitive Lipase to LDs, generating maximal lipolysis (Granneman, et al. 2009; Sztalryd, et al. 2003). In addition to their role in adipocyte biology, lipid droplets have been implicated in foam cell formation in atherosclerosis, hepatitis C virus replication, liver steatosis and cancer cell survival (Bensaad, et al. 2014; Qiu, et al. 2015; Reue 2011).

Eutherian mammals have evolved multiple mechanisms to maintain a stable core body temperature. Broadly, these mechanisms minimize heat loss (for example presence of fur, nesting, changes in body posture) and actively increase heat production. In the initial response to a cold environment, mammals significantly increase their metabolic rate and initiate a shivering response. After prolonged cold exposure, they activate non-shivering thermogenic mechanisms which result in cold acclimation (Cannon and Nedergaard 2004; Griggio 1982). Non-shivering thermogenesis depends on heat generation by both brown adipose tissue (BAT) and skeletal muscle (Silva 2011). BAT is characterized by the presence of the mitochondrial UCP1 protein, which uncouples respiratory chain electron transfer from ATP production. This futile cycle dissipates energy as heat and is stimulated by β-adrenergic stimulation and activation of lipolysis (Cannon and Nedergaard 2011). Additionally, non-shivering muscle-based thermogenesis is also known to participate in cold- and diet-induced heat generation, particularly when there is diminished BAT-dependent thermogenesis. For example, Sarcolipin, a regulator of the SERCA (sarcoendoplasmic reticulum (SR) calcium transport ATPase) pump has been shown to promote a futile cycle of ATP hydrolysis by uncoupling ATP hydrolysis from $Ca^{2+}$ pumping back into the SR, resulting in heat

production and protection from diet-induced obesity (Bal, et al. 2012; Maurya, et al. 2015; Smith, et al. 2002).

HILPDA (hypoxia-inducible lipid droplet associated protein) was originally identified as a hypoxia-inducible gene and was named Hypoxia Inducible Gene 2 (HIG2) (Denko, et al. 2000). Later studies confirmed its hypoxic inducibility in different cell contexts (Elvidge, et al. 2006; Wang, et al. 2005). Evolutionary appearance of Hilpda is quite recent, as orthologs of the human gene product are limited to those in other mammals. The lipid droplet localization of Hilpda was determined by Gimm et al, who also showed that its overexpression increases the intracellular accumulation of neutral lipids and cytokine expression in tumor cells (Gimm, et al. 2010). Evidence for the role of Hilpda in organismal physiology has recently emerged through the use of tissue-specific deletion in engineered mouse strains. Genetic manipulation in murine liver has implicated HILPDA in triglyceride accumulation by mechanisms involving PPARα-dependent *Hilpda* induction, triglyceride secretion and regulation of lipolysis, although direct inhibition of lipase activity was not found (DiStefano, et al. 2015; Mattijssen, et al. 2014). Additionally, deletion of *Hilpda* in WAT and/or BAT did not impact lipolysis, despite its robust induction during adipocyte differentiation in vitro and nutritional manipulations in vivo (Dijk, et al. 2017; DiStefano, et al. 2016).

In this work, we investigated the impact of whole body *Hilpda* loss on survival, growth and adaptation to environmental stresses. By using a novel genetically engineered mouse model we have uncovered Hilpda's involvement in thermoregulation and energy expenditure by exposing the animals in stressful environments similar to what would be found outside the climate- and diet controlled laboratory.

## Materials and Methods

### Mouse genetics

A mutant mouse strain where the *Hilpda* gene was knockout and firefly Luciferase was knocked in was generated by Xenogen Biosciences (Cranbury, NJ, USA). BAC clone RP23-104P4 was used for generating homologous arms and southern probes by PCR or RED cloning/gap-repair method. The final vector was obtained by standard molecular cloning methods and linearized before electroporation into C57BL/6-Tac ES cells. The targeted ES cells were injected into FVB blastocysts and chimeras were mated to WT C57BL/6-Tac females. We received mice at N3, F5 and back-crossed them to sequentially to both C57BL/6-Tac and C57BL/6J animals for a total of 6 generations. For genotyping we used a triplex PCR with primers: 53F: 5′-CCTGGGCTACATAGCAGGGAGAGG-3′, KOR: 5′-GATGCCCAGCACATAGAGGTTCAGC-3′ and Luc-R: 5′-CTCCAGCGGTTCCATCTTCCAGC-3′. Mouse chow was from Teklad (#LM-485), with the following caloric composition: carbohydrates 58%, protein 25% and fat 17%. Euthanasia was performed by $CO_2$ inhalation followed by cervical dislocation. All animal studies were approved by the Institutional Animal Care and Use Committee (IACUC) of The Ohio State University, in accordance with the National Institutes of Health guide for the care and use of Laboratory animals.

### Metabolic cage measurements

Whole animal metabolic parameters were measured using the Comprehensive Lab Animal Monitoring System (CLAMS) equipped with a temperature-controlled environmental chamber from Columbus Instruments (Columbus, OH, USA). Female, single housed 4–5 month old mice were used for all experiments, unless otherwise indicated. For the work done at 22°C the measurements of the first 24h were excluded from the analysis to allow for acclimation to the new environment. For the experiments performed at 30°C the first 48–60h were excluded in order for brown fat thermogenesis to cease. For body temperature measurements, thermal transponders (IPTT300, Bio Medic Data System, Seaford, DE, USA) were implanted under 2% isofluorane anesthesia subdermally in the interscapular region, attempting to place the transponder directly above the brown adipose tissue. Readings were recorded non-invasively as previously described (Bal et al. 2012). The procedure was minimally invasive and the animals resumed normal activity immediately after recovery from anesthesia.

### Blood and tissue chemistry

To test for glucose tolerance, mice were fasted overnight and 2 g/kg glucose in saline was injected intraperitoneally. Blood was drawn from the tail at 0, 15, 30, 60 and 90min and tested with a ReliOn Ultima glucose meter (Walmart, Bentonville, AR, USA). Fasted serum chemistry analysis was performed by the OSU Comparative Pathology and Phenotyping core facility. Tissue triglyceride content was measured with the Triglyceride Quantification Kit (Abcam, Cambridge, MA, USA) following the manufacturer's instructions.

### In vitro adipocyte differentiation

Stromal vascular fraction (SVF) from interscapular BAT was isolated from 3 WT and 3 Hilpda KO mice between the ages of 4–5 weeks. The isolation buffer contained 123mM NaCl, 5mM KCl, 1.3mM $CaCl_2$, 5mM Glucose, 100mM HEPES, 4% BSA, 1.5 mg/mL Collagenase A (Sigma, St. Louis, MO, USA), 100 U/mL penicillin and 100 μg/mL streptomycin. Cells were expanded in DMEM supplemented with 15% FBS and were used within 2 passages. For SVF differentiation into brown adipocytes 25 X $10^4$ undifferentiated cells were plated in 6-well plates and grown to confluence. The following day growth media was changed to differentiation induction media consisting of DMEM with 10% FBS, 20nM insulin, 1nM T3, 125μM indomethacin, 2 μg/mL dexamethasone and 0.5mM IBMX (all from Sigma, St. Louis, MO, USA). Two days later the induction media were replaced by differentiation maintenance media of DMEM, 10% FBS, 20nM insulin and 1nM T3 for an additional 4–6 days.

### Adipocyte metabolic assays

Brown adipocyte oxygen consumption and mitochondrial function were analyzed in an XF96 Seahorse analyzer (Agilent, Santa Clara, CA, USA). Three independent SVF preparations per genotype were plated onto L-lysine-coated XF96 plates in 5 replicates and differentiated for 6 days as described in section 2.4. Basal oxygen consumption rates (OCR) were measured in maintenance media and uncoupled oxygen consumption was calculated 15min after the injection of 10μM forskolin and 10μM oligomycin. For glycerol release

quantification, day 7 differentiated adipocytes were switched to FBS-free maintenance media for 2h and glycerol concentration in the media was measured with a Glycerol Assay kit (Sigma, St. Louis, MO, USA). The cell monolayers were lysed in protein lysis buffer and total protein content was used to normalize the glycerol release values.

### Establishment and treatment of MEF cell lines

Embryos from *Hilpda* Het X Het crosses were isolated at 13.5 p.c., and the heads and internal organs were removed and used for genotyping. Fibroblasts were isolated by mincing in 0.25% trypsin/EDTA solution. Immortalized cell lines were established by retroviral infection with a pBABE-puro SV40 LT plasmid (from Thomas Roberts through Addgene #13970) and puromycin resistance selection. In vitro hypoxia was achieved in an H35 HypOxystation (HypOxygen, Frederick, MD, USA).

### Western blotting

Cell monolayers and mouse organs were washed in PBS and lysed in radioimmunoprecipitation assay buffer, sonicated and cleared by centrifugation. Protein concentration was measured with a bicinchoninic acid assay kit (ThermoFisher, Waltham, MA, USA). Proteins were separated on Tris-glycine or Tris-tricine gels, transferred onto PVDF membranes and probed with the following primary antibodies: anti-CEBPb (Cell Signaling, Danvers, MA, USA), anti-PPARg and anti-Plin1 (Thermo Scientific, Waltham, MA, USA), anti-pyruvate dehydrogenase E1a (Abcam, Cambridge, MA, USA), anti-tubulin (Santa Cruz, Dallas, TX, USA), or a custom-made anti-Hilpda polyclonal antibody raised against the C-terminus of human Hilpda (Open Biosystems, Huntsville, AL, USA). Primary antibodies were detected with IRDye 680RD and IRDye800CW goat anti-mouse and anti-rabbit secondary antibodies (LI-COR, Lincoln NE, USA), respectively, and infrared signal detected with an Odyssey SA LI-COR imager (Lincoln, NE, USA).

### Bioluminescent Imaging

Mice were injected intraperitoneally with 150mg/kg potassium d-luciferin (PerkinElmer, Waltham, MA, USA) in saline and euthanized 10min later. Organs were quickly removed and imaged in a Xenogen IVIS100 system (PerkinElmer, Waltham, MA, USA).

### Gene expression profiling

Gene expression analysis was performed using RNA from interscapular brown fat of overnight fasted mice (n=4). Briefly, RNA was isolated with Trizol (Thermo Scientific, Waltham, MA, USA). The samples were biotin labeled and hybridized to Affymetrix GeneChip Mouse Transcriptome Array 1.0 platform by the Genomics Shared Resource Facility, The Ohio State University Comprehensive Cancer Center. Normalizations and gene expression changes were analyzed in the Affymetrix Expression Console. The microarray data are deposited with the Gene Expression Omnibus (GEO) with accession number GSE100201.

### Statistical analysis

Data were analyzed with GraphPad Prism 7 (GraphPad Software, Inc., San Diego, CA, USA). Data from 2 groups only were analyzed by unpaired Student's t-test. Metabolic data were analyzed by two-way ANOVA and Fisher's LSD test. Statistical significance was set at $p<0.05$ and data are presented as mean+S.E.M. The number of biological replicates or sample size are indicated in the respective figure legends.

## Results

### Establishment of *Hilpda* KO mice

The mouse *Hilpda* gene contains two exons and is predicted to code for two transcript variants. Our Hilpda KO/reporter strain (hereafter referred to as KO) was generated by replacing the coding sequence of exon 2 with the firefly Luciferase coding sequence (Fig. 1A–B). The KO mice are viable, fertile, and born at the expected Mendelian ratios (data not shown). To map *Hilpda* promoter activity in vivo, we injected adult KO mice with D-luciferin, euthanized them and imaged excised tissues for bioluminescence (Fig. 1C). High luciferase activity was detected in a large number of organs and tissues, including lung, white adipose tissue, liver and intestine. This suggests constitutive promoter activity in organs of diverse functions and/or high activity in stromal components. Western blotting on WT organ lysates showed variable levels of expression, with the highest levels in lung followed by the heart and liver (Figure 1D). To validate the specificity of the polyclonal anti-Hilpda antibody we treated immortalized MEFs from WT and KO embryos with normoxia or 1% $O_2$ hypoxia for 24h. We found significant hypoxic induction of Hilpda in the WT cells and confirmed the complete loss of detectable protein in the KO samples (Fig. 1E). Hilpda loss did not impact body weight gain in female mice fed a standard diet (Fig. 1F), however daily food consumption was decreased in the KO animals (Fig. 1G). This decreased food intake, associated with normal weight gain, raised the possibility of either lower energy expenditure or abnormal nutrient absorption in the absence of Hilpda.

### Altered metabolism in the absence of HILPDA under chronic, mild cold stress

To characterize possible metabolic alterations by the complete genetic ablation of *Hilpda* we measured basal metabolic parameters of adult, female mice maintained in standard housing temperatures (22°C). The KO animals had lower oxygen consumption, voluntary physical activity, as well as energy expenditure throughout the light cycle (Fig. 2A–C). Further analysis of our metabolic cage data showed that the significantly lower total activity in the KO mice was attributed to both lower ambulatory activity in the X plane and lower Z plane breaks (rearing activity) (data not shown). We did not measure appreciable changes in the respiratory exchange ratio (RER) (Fig. 2D). This indicates an overall reduced metabolism without a shift in the relative contribution of carbohydrate and fat oxidation.

### Thermoneutrality abolishes the *Hilpda* KO phenotype

The reduced oxygen consumption at 22°C in conjunction with reduced ambulatory activity in the *Hilpda* KO mice raised the possibility of an adaptive change in the relative contribution of brown fat and muscle towards the maintenance of normal body temperature.

In order to dissociate the two, we acclimatized WT and KO animals to thermoneutrality (30°C) to minimize BAT activation and performed indirect calorimetry (Fig. 2E–H). As expected, average oxygen consumption and energy expenditure of both genotypes was lower compared to 22°C, since the energetic requirement for heat production was minimal. Interestingly, thermoneutrality eliminated the differences in oxygen consumption and in physical activity seen at regular housing temperatures, suggesting that Hilpda participates in homeostatic mechanisms at ambient temperatures.

## Hilpda is upregulated early during differentiation in vitro

Previous reports have shown that Hilpda is expressed in human and murine adipocytes and responds to PPAR- and b-adrenergic signaling (Dijk et al. 2017; DiStefano et al. 2016). To determine the regulation of Hilpda expression and its impact on adipocyte differentiation in our genetically engineered model we isolated the stromal vascular fraction (SVF) from interscapular BAT and differentiated it *in vitro* (Fig. 3). First, we followed the changes in protein levels of known transcriptional regulators and adipocyte markers over time, in order to reveal any possible impact of *Hilpda* ablation on the differentiation cascade (Fig. 3A). We detected early and transient upregulation of CEBP/b by day 1 in both genotypes, followed by the appearance of PPARg and at later time points increases in Plin1, UCP1 and the E1a subunit of the mitochondrial enzyme Pyruvate Dehydrogenase also in both genotypes. We concluded that the hormonal response, adipogenic program and expression of brown fat-specific markers, like mitochondrial biogenesis and UCP1 expression, are not impaired in the *Hilpda* KO cells. Interestingly, we observed upregulation of Hilpda protein early in the differentiation course, with detectable levels already on day 1. These kinetics differ significantly from those of Plin1 and suggest regulatory mechanisms in addition to the response to PPAR.

Based on the upregulation of Hilpda during the induction phase of differentiation, we hypothesized that one or more components of the chemical cocktail were responsible for this acute response. We performed a time course on day 0 preadipocytes incubated either in the full cocktail (insulin, T3, dexamethasone, indomethacin, IBMX) or BAT maintenance media (insulin and T3) plus the individual induction components, and found that IBMX was sufficient to increase HILPDA protein (Fig. 3B). IBMX is a non-specific Phosphodiesterase inhibitor, suggesting that elevation in cyclic nucleotide levels positively regulate HILPDA. Moreover, when day 7 adipocytes were activated with 10μM forskolin to mimic b-adrenergic signaling, we observed an additional accumulation of HILPDA (Fig. 3C), further supporting its regulation by cAMP. We also probed forskolin-treated samples for Plin1 as a control for forskolin's activity, which caused a shift in the electrophoretic mobility of Plin1. This is consistent with the phosphorylation of Plin1 by PKA during the stimulation of lipolysis (Greenberg, et al. 1991).

## Hilpda KO brown adipocytes are functional

Next, we performed a functional characterization of *Hilpda* WT (wild type) and KO adipocytes by measuring metabolic parameters. Oxygen consumption rates, degree of uncoupled mitochondrial oxygen consumption as well as basal glycerol release rates were similar between the groups, showing that Hilpda is not necessary for mitochondrial fuel

oxidation or triglyceride hydrolysis, at least in the presence of high levels of nutrients (Fig. 3D–F). Consistent with our in vitro findings, *Hilpda* KO mice were able to increase their metabolism compared to ambient temperature (Fig, 4A–D) and defend body temperature when exposed to cold acutely for 6h (Fig. 4E). Interestingly, following the stress, the KO mice increased their food intake compared to the WT (Fig. 4F)

### Hilpda participates in thermoregulation during fasting

The ability of the *Hilpda* KO mice to thermoregulate in the fed state prompted us to introduce an additional stressor and subject them to fasting, another physiologic condition that induces lipid store mobilization and systemic changes in metabolism. Following food deprivation during the dark phase for 12h at 22°C, the KO mice had significantly lower body temperature than the WT (Fig. 5A). The defect became more severe when the fasting was followed by exposure to cold (Fig. 5B). To identify genes whose expression may be deregulated in the absence of Hilpda and could be responsible for this phenotype, we performed microarray gene expression analysis on brown fat from fasted mice. Statistical analysis of the data using as cutoff values a 2-fold difference between genotypes, with $p<0.01$ and FDR 0.05 did not yield any candidates regulated by the *Hilpda* status. A curated list of select genes associated with BAT function is shown in table 1. This result leads us to conclude that the hypothermia of the Hilpda KO animals cannot be traced to gene expression changes in the BAT.

Liver- and adipose-specific *Hilpda* deletion has been reported to improve glucose tolerance (DiStefano et al. 2015; DiStefano et al. 2016). The glucose tolerance test after 16h of overnight fasting in our whole-body KO model showed a trend towards higher glucose peak levels in the absence of Hilpda but it did not reach statistical significance (Fig. 5C). We performed fasting serum lipid analysis to test if Hilpda loss would alter systemic lipid mobilization, either as lipid release or as uptake to and from the bloodstream and found higher levels of HDL in the KO mice, while triglycerides, cholesterol, LDL, CK and LDH levels were unaltered (Table 2). Additionally, we measured the animals' metabolism during fasting (Fig. 6A–D). Oxygen consumption and energy expenditure were lower in the KO group during the active phase of the daily cycle and physical activity was decreased throughout the experiment. The respiratory exchange ratio was not different between the groups similar to what we had observed in the fed state. Finally, triglyceride content in WAT, liver and gastrocnemius muscles of fasted mice was not affected by the *Hilpda* status (Fig. 6E–G).

## Discussion

Here we present the generation and metabolic characteristics of a *Hilpda* whole animal knockout mouse model. We found that Hilpda is not required for viability, growth and reproduction. At standard housing temperatures the Hilpda KO mice had reduced metabolism, consuming less oxygen, being less active and expending less energy. Concomitantly, their food intake was lower, a finding that can explain their normal weight gain. Our result that thermoneutrality diminishes these metabolic differences suggests that thermoregulatory mechanisms have undergone adaptations in the absence of HILPDA. Our

data also suggest that if any of these adaptations involve the brown adipose tissue, they do not include changes at the level of gene transcription. This is in agreement with previous reports who were unable to find significant gene expression changes in tissue-specific Hilpda KO models (DiStefano et al. 2015; Mattijssen et al. 2014).

It is possible that the primary impact of Hilpda is on locomotor activity, either at the level of muscle contractility or by other neurological, behavioral or hormonal mechanism(s). These may, for example, include compensations such as change in body posture and blood flow or changes in skeletal muscle thermogenesis through uncoupling of the SERCA pump by Sarcolipin (Rowland, et al. 2015). It is also possible that, in our genetic background, BAT function below thermoneutrality is altered when Hilpda is absent, similar to what has been seen in the adipose tissue-specific KO model (Dijk et al. 2017; DiStefano et al. 2016) In agreement with recently published reports, we did not find a cell-autonomous defect of HILPDA KO adipocytes in their differentiation capacity or lipolysis (Dijk et al. 2017; DiStefano et al. 2016). Hilpda was, however, required for body temperature defense after fasting, and the hypothermia of the KO mice was associated with rebound hyperphagia. Adipose tissue-specific, and also liver-specific deletion of *Hilpda* has been shown to improve glucose tolerance in male mice (DiStefano et al. 2015). Females from the whole body KO strain did not show a similar phenotype and fasting liver triglyceride content was not significantly decreased. Although the possibility of gender-, sub strain- or diet-specific phenotypes cannot be ruled out, our results raise the possibility that the simultaneous deletion of *Hilpda* in all tissues re-equilibrates lipid droplet trafficking.

Hilpda's first identified gene expression inducer was hypoxia (Denko et al. 2000), a finding that we confirmed here in immortalized MEFs. It is now evident that additional stresses and transcription factors, such as PPARs, cAMP and nutrient imbalance induce Hilpda expression (this work) and (Dijk et al. 2017; DiStefano et al. 2015; DiStefano et al. 2016; Gimm et al. 2010; Mattijssen et al. 2014; Wang, et al. 2010). The mechanistic details of Hilpda-dependent lipid accumulation are not known yet and require additional biochemical investigation. An intriguing characteristic of Hilpda is the lack of any significant similarity between this short 63–64aa protein and other more ancient proteins, despite the presence of lipid storage organelles in all eukaryotes. Based on this paucity of annotated functional domains, we propose that Hilpda functions as a docking site or as a regulatory component of larger complex(es) that control lipid droplet dynamics. Furthermore, the implication of Hilpda in thermoregulation, given the relatively recent evolutionary emergence of the gene, makes it reasonable to propose that Hilpda serves to enhance some unique aspects of the mammalian fitness that are absent from other classes in the Animal Kingdom.

Emerging evidence shows that more than one mechanism, possibly via different protein interactions, may dictate complementary routes to the end point of lipid droplet growth. In support of this model, Hilpda has been reported to negatively regulate lipolysis and triglyceride secretion in the liver, but not in adipose tissue (Dijk et al. 2017; DiStefano et al. 2015; DiStefano et al. 2016; Mattijssen et al. 2014). Cell-context and the particular lipid droplet proteome may also determine distinct ways of lipid ester storage dynamics (Beller, et al. 2008; Guo, et al. 2008; Khor, et al. 2014) and therefore the significance of Hilpda in these processes.

In conclusion, we found that genetic deletion of *Hilpda* decreases physical activity and energy expenditure and sensitizes mice to fasting-induced hypothermia.

## Acknowledgments

**Funding**

Funded by CA191653 (I.P.), CA197713 (A.J.G.), CA067166 (A.J.G. and N.C.D.) and DK105109 (K.I.S). The OSUCCC shared resources are supported by a Cancer Center Support Grant (CA016058). NIH had no role in the study design, data generation, the writing of this report or the decision to submit it for publication.

## References

Bal NC, Maurya SK, Sopariwala DH, Sahoo SK, Gupta SC, Shaikh SA, Pant M, Rowland LA, Bombardier E, Goonasekera SA, et al. Sarcolipin is a newly identified regulator of muscle-based thermogenesis in mammals. Nat Med. 2012; 18:1575–1579. [PubMed: 22961106]

Beller M, Sztalryd C, Southall N, Bell M, Jackle H, Auld DS, Oliver B. COPI complex is a regulator of lipid homeostasis. PLoS Biol. 2008; 6:e292. [PubMed: 19067489]

Bensaad K, Favaro E, Lewis CA, Peck B, Lord S, Collins JM, Pinnick KE, Wigfield S, Buffa FM, Li JL, et al. Fatty acid uptake and lipid storage induced by HIF-1alpha contribute to cell growth and survival after hypoxia-reoxygenation. Cell Rep. 2014; 9:349–365. [PubMed: 25263561]

Cannon B, Nedergaard J. Brown adipose tissue: function and physiological significance. Physiol Rev. 2004; 84:277–359. [PubMed: 14715917]

Cannon B, Nedergaard J. Nonshivering thermogenesis and its adequate measurement in metabolic studies. J Exp Biol. 2011; 214:242–253. [PubMed: 21177944]

Denko N, Schindler C, Koong A, Laderoute K, Green C, Giaccia A. Epigenetic regulation of gene expression in cervical cancer cells by the tumor microenvironment. Clin Cancer Res. 2000; 6:480–487. [PubMed: 10690527]

Dijk W, Mattijssen F, de la Rosa Rodriguez M, Loza Valdes A, Loft A, Mandrup S, Kalkhoven E, Qi L, Borst JW, Kersten S. Hypoxia-inducible lipid droplet-associated (HILPDA) is not a direct physiological regulator of lipolysis in adipose tissue. Endocrinology. 2017

DiStefano MT, Danai LV, Roth Flach RJ, Chawla A, Pedersen DJ, Guilherme A, Czech MP. The Lipid Droplet Protein Hypoxia-inducible Gene 2 Promotes Hepatic Triglyceride Deposition by Inhibiting Lipolysis. J Biol Chem. 2015; 290:15175–15184. [PubMed: 25922078]

DiStefano MT, Roth Flach RJ, Senol-Cosar O, Danai LV, Virbasius JV, Nicoloro SM, Straubhaar J, Dagdeviren S, Wabitsch M, Gupta OT, et al. Adipocyte-specific Hypoxia-inducible gene 2 promotes fat deposition and diet-induced insulin resistance. Mol Metab. 2016; 5:1149–1161. [PubMed: 27900258]

Elvidge GP, Glenny L, Appelhoff RJ, Ratcliffe PJ, Ragoussis J, Gleadle JM. Concordant regulation of gene expression by hypoxia and 2-oxoglutarate-dependent dioxygenase inhibition: the role of HIF-1alpha, HIF-2alpha, and other pathways. J Biol Chem. 2006; 281:15215–15226. [PubMed: 16565084]

Fujimoto T, Parton RG. Not just fat: the structure and function of the lipid droplet. Cold Spring Harb Perspect Biol. 2011:3.

Gimm T, Wiese M, Teschemacher B, Deggerich A, Schodel J, Knaup KX, Hackenbeck T, Hellerbrand C, Amann K, Wiesener MS, et al. Hypoxia-inducible protein 2 is a novel lipid droplet protein and a specific target gene of hypoxia-inducible factor-1. FASEB J. 2010; 24:4443–4458. [PubMed: 20624928]

Goodman JM. The gregarious lipid droplet. J Biol Chem. 2008; 283:28005–28009. [PubMed: 18611863]

Granneman JG, Moore HP, Krishnamoorthy R, Rathod M. Perilipin controls lipolysis by regulating the interactions of AB-hydrolase containing 5 (Abhd5) and adipose triglyceride lipase (Atgl). J Biol Chem. 2009; 284:34538–34544. [PubMed: 19850935]

Greenberg AS, Egan JJ, Wek SA, Garty NB, Blanchette-Mackie EJ, Londos C. Perilipin, a major hormonally regulated adipocyte-specific phosphoprotein associated with the periphery of lipid storage droplets. J Biol Chem. 1991; 266:11341–11346. [PubMed: 2040638]

Griggio MA. The participation of shivering and nonshivering thermogenesis in warm and cold-acclimated rats. Comp Biochem Physiol A Comp Physiol. 1982; 73:481–484. [PubMed: 6128133]

Guo Y, Walther TC, Rao M, Stuurman N, Goshima G, Terayama K, Wong JS, Vale RD, Walter P, Farese RV. Functional genomic screen reveals genes involved in lipid-droplet formation and utilization. Nature. 2008; 453:657–661. [PubMed: 18408709]

Hsieh K, Lee YK, Londos C, Raaka BM, Dalen KT, Kimmel AR. Perilipin family members preferentially sequester to either triacylglycerol-specific or cholesteryl-ester-specific intracellular lipid storage droplets. J Cell Sci. 2012; 125:4067–4076. [PubMed: 22685330]

Khor VK, Ahrends R, Lin Y, Shen WJ, Adams CM, Roseman AN, Cortez Y, Teruel MN, Azhar S, Kraemer FB. The proteome of cholesteryl-ester-enriched versus triacylglycerol-enriched lipid droplets. PLoS One. 2014; 9:e105047. [PubMed: 25111084]

Krahmer N, Hilger M, Kory N, Wilfling F, Stoehr G, Mann M, Farese RV Jr, Walther TC. Protein correlation profiles identify lipid droplet proteins with high confidence. Mol Cell Proteomics. 2013; 12:1115–1126. [PubMed: 23319140]

Mattijssen F, Georgiadi A, Andasarie T, Szalowska E, Zota A, Krones-Herzig A, Heier C, Ratman D, De Bosscher K, Qi L, et al. Hypoxia-inducible lipid droplet-associated (HILPDA) is a novel peroxisome proliferator-activated receptor (PPAR) target involved in hepatic triglyceride secretion. J Biol Chem. 2014; 289:19279–19293. [PubMed: 24876382]

Maurya SK, Bal NC, Sopariwala DH, Pant M, Rowland LA, Shaikh SA, Periasamy M. Sarcolipin Is a Key Determinant of the Basal Metabolic Rate, and Its Overexpression Enhances Energy Expenditure and Resistance against Diet-induced Obesity. J Biol Chem. 2015; 290:10840–10849. [PubMed: 25713078]

Qiu B, Ackerman D, Sanchez DJ, Li B, Ochocki JD, Grazioli A, Bobrovnikova-Marjon E, Diehl JA, Keith B, Simon MC. HIF2alpha-Dependent Lipid Storage Promotes Endoplasmic Reticulum Homeostasis in Clear-Cell Renal Cell Carcinoma. Cancer Discov. 2015; 5:652–667. [PubMed: 25829424]

Reue K. A thematic review series: lipid droplet storage and metabolism: from yeast to man. J Lipid Res. 2011; 52:1865–1868. [PubMed: 21921134]

Rowland LA, Bal NC, Periasamy M. The role of skeletal-muscle-based thermogenic mechanisms in vertebrate endothermy. Biol Rev Camb Philos Soc. 2015; 90:1279–1297. [PubMed: 25424279]

Silva JE. Physiological importance and control of non-shivering facultative thermogenesis. Front Biosci (Schol Ed). 2011; 3:352–371. [PubMed: 21196381]

Smith WS, Broadbridge R, East JM, Lee AG. Sarcolipin uncouples hydrolysis of ATP from accumulation of Ca2+ by the Ca2+-ATPase of skeletal-muscle sarcoplasmic reticulum. Biochem J. 2002; 361:277–286. [PubMed: 11772399]

Sztalryd C, Kimmel AR. Perilipins: lipid droplet coat proteins adapted for tissue-specific energy storage and utilization, and lipid cytoprotection. Biochimie. 2014; 96:96–101. [PubMed: 24036367]

Sztalryd C, Xu G, Dorward H, Tansey JT, Contreras JA, Kimmel AR, Londos C. Perilipin A is essential for the translocation of hormone-sensitive lipase during lipolytic activation. J Cell Biol. 2003; 161:1093–1103. [PubMed: 12810697]

Wang V, Davis DA, Haque M, Huang LE, Yarchoan R. Differential gene up-regulation by hypoxia-inducible factor-1alpha and hypoxia-inducible factor-2alpha in HEK293T cells. Cancer Res. 2005; 65:3299–3306. [PubMed: 15833863]

Wang X, Bjorklund S, Wasik AM, Grandien A, Andersson P, Kimby E, Dahlman-Wright K, Zhao C, Christensson B, Sander B. Gene expression profiling and chromatin immunoprecipitation identify DBN1, SETMAR and HIG2 as direct targets of SOX11 in mantle cell lymphoma. PLoS One. 2010; 5:e14085. [PubMed: 21124928]

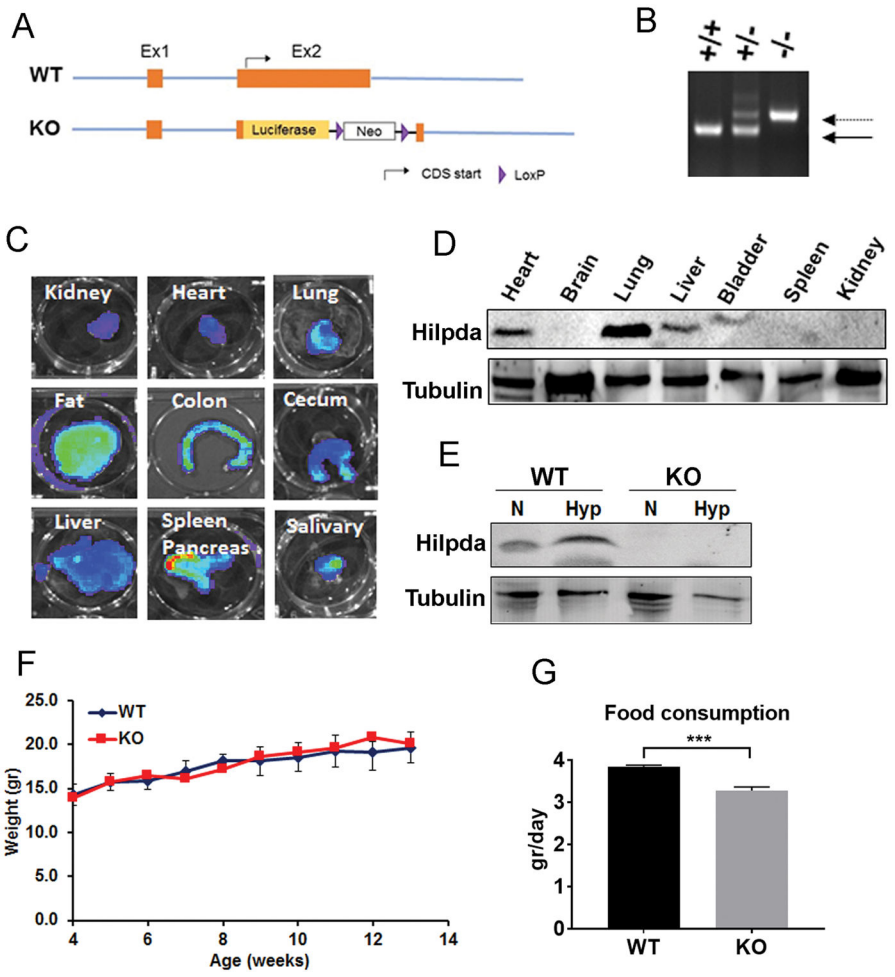


**Figure 1.**

Generation of HILPDA KO mice. A) Schematic of the murine *Hilpda* gene and the designed knockout/reporter allele. B) Representative image of genotyping PCR products of *Hilpda* WT (+/+), heterozygous (+/−) and KO (−/−) animals. Solid arrow: wild type product 0.32kb, dashed arrow: knockout product 0.39kb (C) Bioluminescent detection of *Hilpda* promoter activity in a KO mouse after injection of 0.1mg/mouse D-Luciferin followed by euthanasia 10min later. **D)** Hilpda protein expression in the indicated organs of a fed female mouse. E) Immortalized mouse embryonic fibroblasts were treated in vitro with normoxia (N) or 1% $O_2$ (Hyp) for 24h and Hilpda protein levels were detected by western blotting. F) Body weight curves of group housed female mice between the ages of 4 and 13 weeks (n=7). G) Daily food consumption of single housed female mice (n=5) (*** $p<0.0001$ by Student's t test).

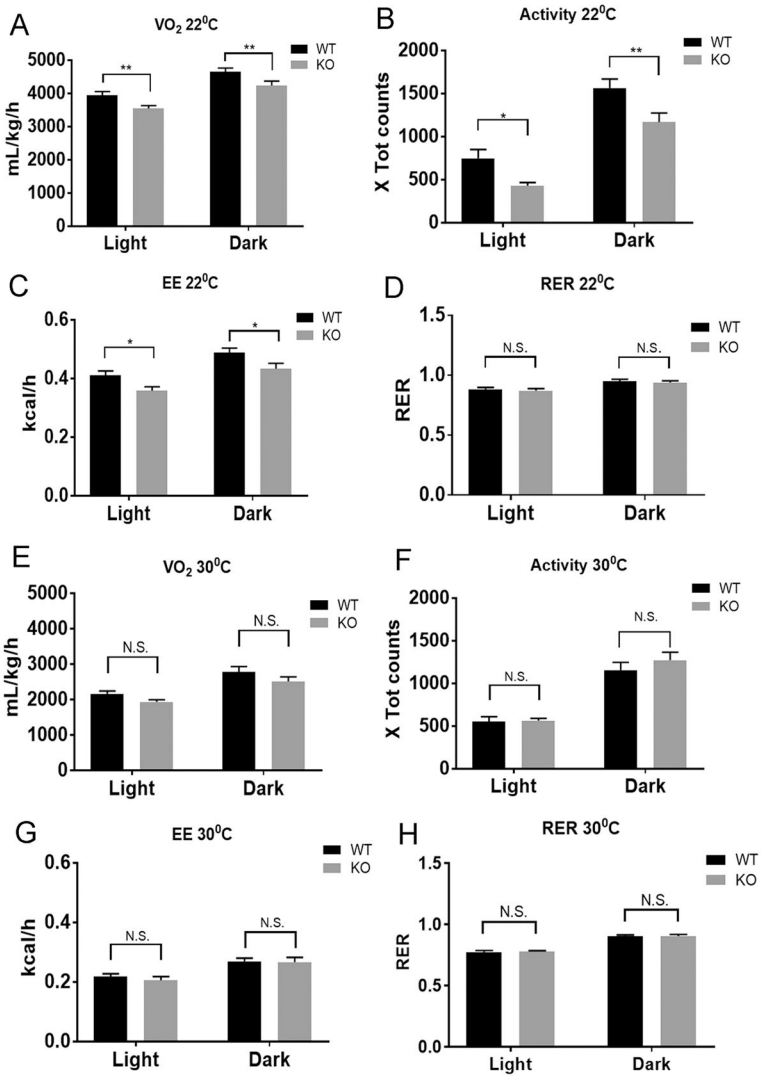


**Figure 2.**

*Hilpda* ablation reduces whole metabolism at 22°C but not at 30°C. A–D) Metabolic parameters of individually housed, fed, female 4–5 month old mice were measured in metabolic cages following a 24h acclimation period. A) average $VO_2$ consumption B) physical activity, C) energy expenditure, D) respiratory exchange ratio (n=16). E–H) Metabolic parameter analysis of fed female mice at thermoneutrality following 48–60h acclimation. E) average $VO_2$ consumption, F) physical activity, G) energy expenditure, H) respiratory exchange ratio (n=12–15). Light: 7am–7pm, dark: 7pm–7am. (*p<0.05, **p<0.01, N.S. not significant by two-way ANOVA and Fisher's LSD test). Error bars: S.E.M.

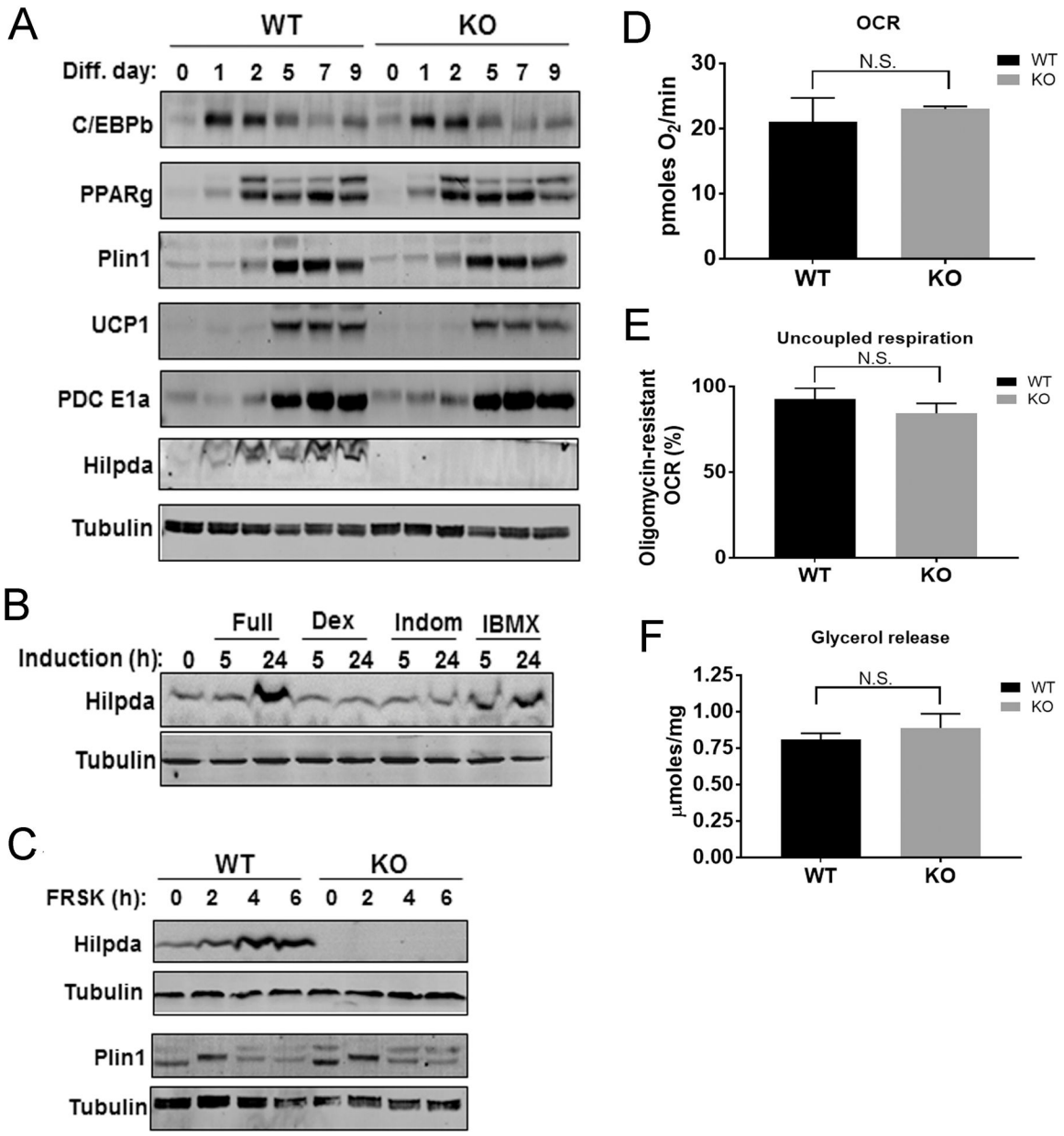


**Figure 3.**

Upregulation of Hildpa during BAT differentiation and activation in vitro. A) Time course of adipocyte markers' protein levels during the differentiation of stromal vascular fraction isolated from the interscapular brown fat of 4 week old mice. Day 0 corresponds to confluent cell cultures before the addition of the induction cocktail. Representative images of 2 independent SVF preparations are shown. B) Western blot of Hilpda protein in early time points during differentiation. Day 0 preadipocytes were incubated in BAT maintenance media plus the complete induction cocktail (2 µg/mL dexamethasone, 125 µM indomethacin, 0.5mM IBMX) or maintenance media plus individual inducers for 5- or 24h. C) Protein levels of Hilpda and Plin1 on day 7 brown adipocytes after 10 µM forskolin treatment for the indicated time points. D–F) Brown adipocyte metabolism in vitro: D) oxygen consumption

rates. E) proton leak as determined by oxygen consumption resistant to 10 μM Forskolin/Oligomycin (n=3). F) basal glycerol release per mg of protein. Adipocytes were switched to serum-free media for 2h and the supernatant was analyzed for glycerol content. The cell monolayer was lysed in RIPA buffer and total protein content was used for normalizations (n=3).

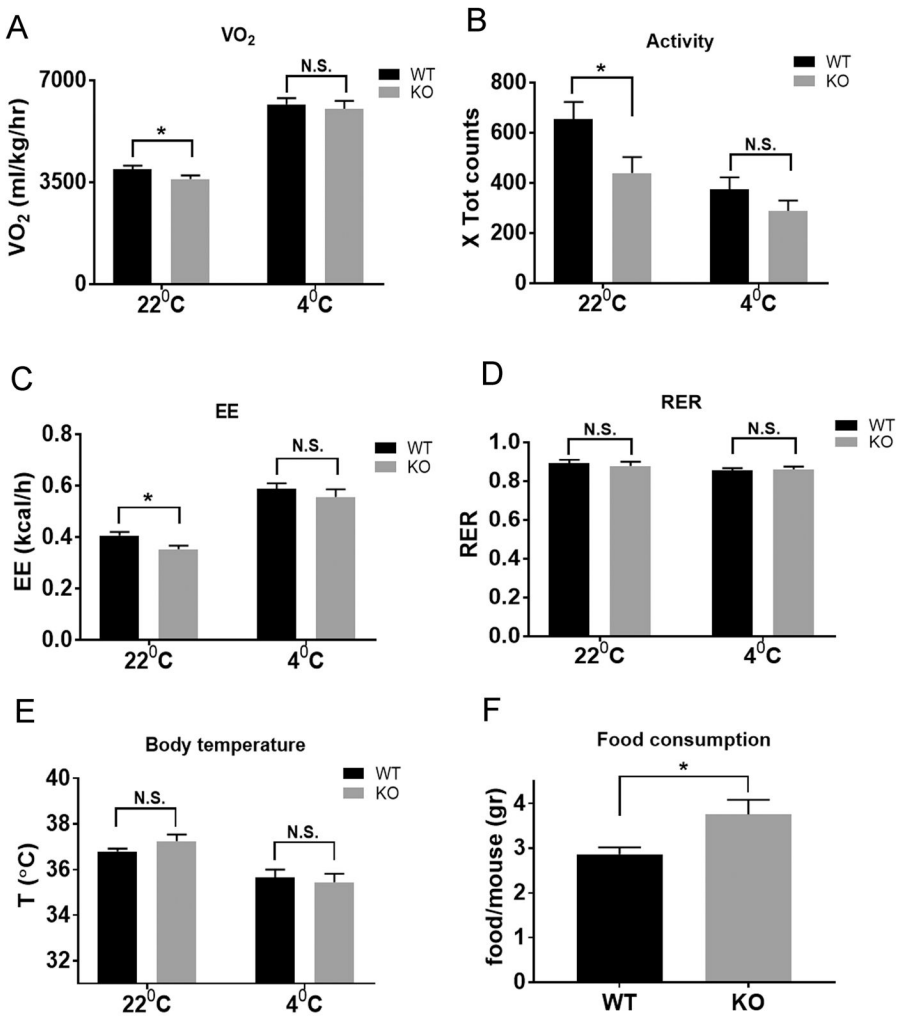


**Figure 4.**

Metabolic parameters of fed, female mice during acute cold exposure. Animals were acclimatized in the metabolic cages at 22°C for 48h and the temperature was dropped to 4°C during the light cycle for 6h. The 22°C data correspond to 6h of the light cycle on the day before the cold exposure. A) average $VO_2$ consumption B) physical activity, C) energy expenditure, D) respiratory exchange ratio (n=11–13). E) body temperature measured by implanted thermotransponders at the beginning and the end of cold exposure. (n=5), F) food consumption for the first 24h after the end of the cold exposure (n=5). Error bars: S.E.M. (* $p<0.05$, N.S: not significant by Student's t-test)

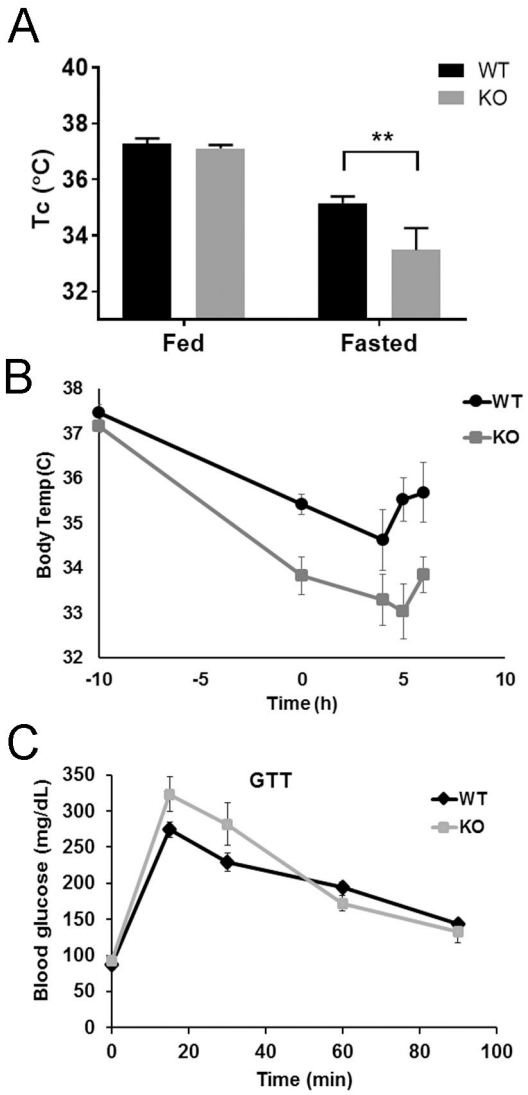


**Figure 5.**

Hilpda-dependent responses to fasting. A) 4–5 month old female mice were implanted subdermally in the interscapular area with thermotransponders and recovered for at least 4 days. Food was removed in the evening and temperatures were recorded 12h later (n=14–16). B) Mice implanted with thermotransponders were fasted as described above during the dark phase at 22°C and the following morning the temperature was dropped to 4°C (t=0 on the graph) for an additional 6h. (n=8) C) Glucose tolerance test after an overnight fast and intraperitoneal injection of 2g/kg glucose (n=7).

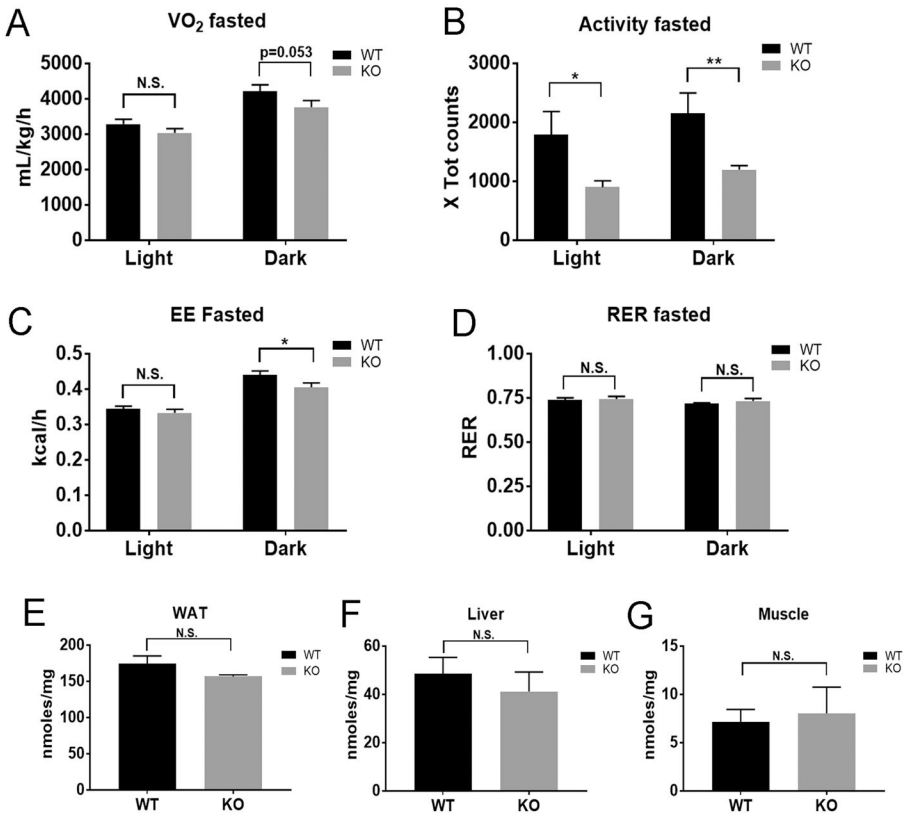


**Figure 6.**

Metabolic responses to fasting. Female mice were single-housed in the metabolic cages for 24–36h and food was removed at 8am for 24h. A) average $VO_2$ consumption, B): physical activity, C) energy expenditure, D) respiratory exchange ratio. E–G) Triacylglycerol content in tissues of fasted female mice. E) white adipose tissue, F) liver G) gastrocnemius muscle (n=4–12) Light: 8:30am–7pm, dark: 7pm–7am (n=9, *p<0.05, **p<0.01, N.S. not significant by two-way ANOVA and Fisher's LSD test).

**Table 1**

Log2 transformed expression levels of representative genes in *Hilpda* WT and KO BAT of overnight fasted mice (n=4)

| Gene | Hilpda WT (log2 aver. signal) | Hilpda KO (log2 aver. signal) |
|---|---|---|
| Plin1 | 15.76 | 14.89 |
| Plin2 | 17.49 | 17.05 |
| Pparg | 16.17 | 16.06 |
| Ucp1 | 19.93 | 19.93 |
| Ppargc1a | 13.60 | 13.91 |
| Ppargc1b | 10.94 | 10.43 |
| Lipe | 15.39 | 15.03 |
| Pnpla2 | 19.56 | 19.55 |
| Adrb3 | 9.47 | 9.06 |

**Table 2**

Fasted serum parameters of female Hilpda WT and KO mice (n=5). p value: Student's unpaired two-tailed t-test

| | WT (mean +/− S.E.M.) | KO (mean +/− S.E.M.) | p value |
|---|---|---|---|
| Cholesterol (mg/dL) | 79.9 +/− 3.4 | 86.1 +/− 4.2 | 0.27 |
| Creatine Kinase (U/L) | 508.2 +/− 26.0 | 859.4 +/− 169.7 | 0.07 |
| HDL (mg/dL) | 29.8 +/−2.9 | 38.8 +/− 1.6 | 0.02* |
| LDL (mg/dL) | 35.6 +/− 3.6 | 34.6 +/− 2.3 | 0.82 |
| Triglycerides (mg/dL) | 71.4 +/− 5.7 | 62.8 +/− 3.4 | 0.23 |
| Lactate Dehydrogenase (U/L) | 205.8 +/− 34.4 | 261.8 +/− 41.1 | 0.32 |